

Point vortex dynamics within a background vorticity patch

Dezhe Z. Jin and Daniel H. E. Dubin^{a)}

Physics Department, University of California at San Diego, La Jolla, California 92093

(Received 16 May 2000; accepted 5 December 2000)

Recent experiments and simulations have observed that the interaction of strong vortices with a low vorticity background can strongly affect the dynamics of both vortices and background. This paper considers an idealized model of this interaction. The background is treated as a patch of uniform vorticity with a nearly circular shape. The strong vortices are treated as point vortices, and their total circulation λ is assumed to be small compared to that of the background. It is found that Kelvin waves on the boundary of the background patch can be driven to large amplitude by the strong vortices, eventually resulting in wave breaking and filamentation. A multiscale analysis finds that the wave-breaking time scales as $\lambda^{-1} \ln \lambda^{-1}$, in agreement with contour dynamics simulations.

© 2001 American Institute of Physics. [DOI: 10.1063/1.1343484]

I. INTRODUCTION

Two-dimensional (2D) Euler flows are the inviscid limit of 2D incompressible Navier–Stokes flows. They are often used as simple models for large scale geophysical and astrophysical flows, such as the polar vortex, tropical cyclones, ocean eddies, and the Great Red Spot of Jupiter.^{1–5} They are also applicable to many experimental systems,⁶ including strongly magnetized plasmas,⁷ thin layers of electrolyte,⁸ and flows in soap films.⁹

The equation of motion for a 2D Euler flow is

$$\partial_t \omega + \mathbf{u} \cdot \nabla \omega = 0, \quad (1)$$

where $\mathbf{u}(\mathbf{r}, t)$ is the velocity field, and

$$\omega(\mathbf{r}, t) = \hat{\mathbf{z}} \cdot \nabla \times \mathbf{u} \quad (2)$$

is the vorticity field. Here $\hat{\mathbf{z}}$ is the unit vector perpendicular to the plane of the flow, and $\mathbf{r} = (x, y)$ is the position vector in the plane. The flow is incompressible:

$$\nabla \cdot \mathbf{u} = 0; \quad (3)$$

therefore, a stream function $\psi(\mathbf{r}, t)$ can be related to the velocity field

$$\mathbf{u} = \nabla \times \psi \hat{\mathbf{z}}. \quad (4)$$

Substituting Eq. (4) into Eq. (2), we obtain Poisson's equation

$$\nabla^2 \psi = -\omega. \quad (5)$$

Two-dimensional Euler flows often contain strong vortices (localized patches of intense vorticity) moving through a low diffuse vorticity background. For example, such structures are observed to form spontaneously in experiments and numerical simulations of freely relaxing 2D turbulence.^{8,10–12} The interaction between the strong vortices and the background vorticity plays an important role in the evolution of these flows. Local mixing of the background by the strong vortices can cause the vortices to move up or

down the local background vorticity gradient;¹³ global mixing of the background can cause the vortices to settle into equilibrium patterns, termed “vortex crystals.”^{12,14,15}

In this paper, we study the interaction between the strong vortices and the background flow with a simple model. The model consists of several point vortices and an extended vortex patch (which represents the low vorticity background). The point vortices are inside the vortex patch, and the flow is subject to a free-space boundary condition (i.e., there are no surrounding boundaries). Lansky *et al.* have studied a similar model in which one point vortex is placed outside of the nearly circular vortex patch. They showed that the point vortex can merge into the vortex patch through successive resonances.¹⁶ Here we concentrate on the case where the point vortices are already inside the patch, and the patch is nearly circular initially.

The dynamics of a collection of point vortices and the dynamics of a vortex patch have separately received considerable attention. For a collection of point vortices, the equilibrium patterns have been exhaustively studied, and stability properties have also been determined.^{17,18} The dynamics of the system is Hamiltonian and is chaotic in most cases.¹⁹

The equilibrium and dynamics of an isolated vortex patch have also been thoroughly examined. For example, it is known that a vortex patch has infinitely many rotating equilibria, among which the circular shape (so called Rankine patch) is the most fundamental.²⁰ The circular patch supports steadily propagating infinitesimal perturbations, or Kelvin waves, on its boundary. Contour dynamics has been used extensively to study the evolution of small disturbances added to equilibrium vortex patches.²¹ Filamentation, or the formation of filaments of vorticity drawn off the vortex patch, often results from the growth of linearly unstable Kelvin waves.²² Numerical and analytical evidence is also present for long time filamentation of arbitrarily small, linearly stable disturbances.²³

Our paper combines the problems of point vortex dynamics and patch dynamics. We concentrate on the limit in which the contour of the vortex patch is nearly circular, and

^{a)}Electronic mail: dhudubin@ucsd.edu

the total circulation of the point vortices is much smaller than that of the vortex patch. This ordering introduces a small parameter λ , the ratio of the average circulation of the point vortices to that of the patch. We evaluate the dynamics analytically using a two-time scale analysis and a novel pseudoenvelope equation based on the high spatial Fourier harmonics of the patch contour. We then compare the results of the analysis to contour dynamics²⁴ simulations. Our analytic approach yields several new results, verified by the simulations. First, we show that the interaction of the strong vortices with free-streaming Kelvin waves on the vortex patch eventually causes wave breaking and filamentation of the patch. We find that when a vortex is within a small distance of the edge of the patch, of order λ^ξ times the patch radius, filamentation occurs rapidly, within one rotation period of the patch. The exponent ξ is found from contour dynamics simulations to be approximately 0.566. For vortices far from the edge of the patch, the time required for waves to break is much longer, scaling as the patch rotation period times $\lambda^{-1} \ln \lambda^{-1}$. (This scaling has recently been verified in a set of 2D fluid experiments using a nonneutral plasma as the working fluid.)²⁵

We also show that, before wave breaking occurs, the dynamics of the point vortices is identical to the dynamics of point vortices within a fixed cylinder of the same radius as the patch and with a free-slip boundary condition, except for an overall rotation caused by the patch and a fast jitter motion caused by Kelvin waves on the patch. Therefore, all results of point vortex dynamics in a circular boundary can be readily applied to the dynamics of the point vortices. For example, we know right away the equilibrium patterns of the point vortices; we know that the Havelock instability²³ applies to these equilibrium patterns—the point vortices cannot be too close to the contour of the vortex patch, otherwise they will be attracted toward the contour, and the equilibrium pattern will be unstable; we also know that the dynamics of the point vortices is in general chaotic.

In Sec. II, we define the model and the perturbation limit, and we discuss the units used in the paper. In Sec. III A, we derive the general nonlinear equations of motion for the model and in Sec. III B we Taylor expand these equations in powers of λ . In Sec. III C, we transform the equation for the patch dynamics into Fourier space. In Sec. IV A, we consider the linearized version of our equations, both as a check on our analysis and in order to determine linear equations for the evolution of the Kelvin waves. In Secs. IV B–IV D, we perform a two-timescale analysis of the nonlinear equations. In Sec. IV D we then introduce a novel “pseudoenvelope” formulation of the patch dynamics in order to determine the filamentation timescale. In Sec. IV E, filamentation is examined in detail for two cases: a single point vortex in the patch, and two equal-strength point vortices in the patch. Throughout Sec. IV, we compare our results to contour dynamics simulations. Finally in Sec. V, we discuss several outstanding questions. A constant of the motion for the slow-time nonlinear dynamics of the Kelvin waves is derived in the Appendix.

II. THE MODEL

The model we consider consists of M point vortices inside a vortex patch. The flow is subject to a free-space boundary condition: $\mathbf{v}(\mathbf{r}) \rightarrow 0$ as $\mathbf{r} \rightarrow \infty$. The positions of the point vortices are $\mathbf{R}_m(t)$, and their circulations are Γ_m , with $m = 1, \dots, M$. The vortex patch has a constant (positive) vorticity ω_0 , and its shape is specified by a smooth single valued function $r_c(\theta, t)$, which is the radial position of the boundary point at polar angle θ at time t . A generic point in the plane is denoted as $\mathbf{r} = (r, \theta)$, where r is the radial position of the point, and θ is the polar angle.

The perturbation limit of the model, which is the main subject of this work, is defined by two conditions. One condition is that the average magnitude of the circulation of the point vortices, $\Gamma_v = (1/M) \sum_m |\Gamma_m|$, is much smaller than the circulation of the vortex patch, $\Gamma = \int d\mathbf{r}^2 \omega_0$, where the region of integration is inside the vortex patch. This defines a small parameter

$$\lambda = \frac{\Gamma_v}{\Gamma}, \quad (6)$$

which we refer as the point vortex strength. The other condition is that the radius of the vortex patch deviates from a circular patch of radius r_b by a small amount $\epsilon(\theta, t)$; furthermore, this deviation compared to the radius of the circular patch is of order λ , i.e.,

$$\left| \frac{\epsilon}{r_b} \right| \sim \lambda. \quad (7)$$

The unperturbed patch has radius r_b , related to Γ and ω_0 by $\Gamma = \pi \omega_0 r_b^2$.

In the perturbation limit $\lambda \ll 1$, there are natural units for the physical quantities. The unit of length is the radius r_b of the unperturbed patch, and the unit of time is $t_0 = 4\pi/\omega_0$, which is the rotation period of the unperturbed patch. Consequently, the unit of velocity is $r_b/t_0 = r_b \omega_0/4\pi$, and that of vorticity is $1/t_0 = \omega_0/4\pi$. Also, the unit of the circulation is $\omega_0 r_b^2/4\pi$, and that of the stream function ψ is $\omega_0 r_b^2/4\pi$.

In these units, the unperturbed patch has radius 1, vorticity 4π , circulation $4\pi^2$, and rotation frequency 2π . In the rest of the paper, these units will be used for the physical quantities and all of the equations will be dimensionless.

III. EQUATIONS OF MOTION

A. General equations

Throughout the rest of this paper, we will work in a frame that rotates with the unperturbed patch rotation frequency 2π . In this rotating frame the evolution equation for the contour of the vortex patch, defined by function $r_c(\theta, t)$, can be derived by considering the motion of a contour point at $\mathbf{r}_c = (r_c, \theta)$. After an infinitesimal time interval dt , the point moves to a new position $\mathbf{r}'_c = (r'_c, \theta')$, where $\theta' = \theta + v_\theta dt/r_c$, and $r'_c(\theta', t+dt) = r_c(\theta, t) + v_r dt$. Here v_r and v_θ are the radial and azimuthal components of the velocity of the boundary point, as seen in the rotating frame. Taylor expanding the above equation to the first order in dt , we obtain

$$\frac{\partial r_c}{\partial t} + \frac{v_\theta}{r_c} \frac{\partial r_c}{\partial \theta} = v_r. \tag{8}$$

The boundary condition for this nonlinear partial differential equation is $r_c(\theta + 2\pi, t) = r_c(\theta, t)$.

The equations of motion for the point vortices are simply given by

$$\frac{d\mathbf{R}_m}{dt} = \mathbf{V}_m, \tag{9}$$

where \mathbf{V}_m is the velocity of the m th point vortex.

To complete the equations of motion, the velocities of the point vortices and the contour points must be calculated. This is done by calculating the stream function ψ , recognizing that the vorticity distribution of the flow is

$$\omega(\mathbf{r}) = \omega_b(\mathbf{r}) + \sum_m \Gamma_m \delta(\mathbf{r} - \mathbf{R}_m) - 4\pi, \tag{10}$$

where the factor of 4π is the vorticity associated with the rotating frame, and

$$\omega_b(\mathbf{r}) = \begin{cases} 4\pi, & \mathbf{r} \text{ inside the vortex patch} \\ 0, & \mathbf{r} \text{ outside the vortex patch} \end{cases} \tag{11}$$

is the vorticity distribution of the vortex patch. Using the free-space Green's function

$$G(\mathbf{r} - \mathbf{r}') = -\frac{1}{2\pi} \ln|\mathbf{r} - \mathbf{r}'|, \tag{12}$$

the solution of Eq. (5) for the stream function is given by

$$\psi = \int d\mathbf{r}'^2 \omega(\mathbf{r}') G(\mathbf{r} - \mathbf{r}') = \psi_b + \psi_v + \pi r^2, \tag{13}$$

where in the second expression we have neglected an unimportant additive constant, and where ψ_b and ψ_v are contributions from the vortex patch and the point vortices, respectively,

$$\psi_b = \int d\mathbf{r}'^2 \omega_b(\mathbf{r}') G(\mathbf{r} - \mathbf{r}'), \tag{14}$$

$$\psi_v = \sum_n \Gamma_n G(\mathbf{R}_n - \mathbf{r}). \tag{15}$$

The velocity at point \mathbf{r} is then determined by Eqs. (5) and (13)

$$\mathbf{v} = \nabla \times \psi \hat{\mathbf{z}} = \mathbf{v}_b + \mathbf{v}_v - 2\pi r \hat{\boldsymbol{\theta}}, \tag{16}$$

where $\mathbf{v}_b = \nabla \psi_b \times \hat{\mathbf{z}}$ is the velocity induced by the vortex patch, and $\mathbf{v}_v = \nabla \psi_v \times \hat{\mathbf{z}}$ is the velocity induced by the point vortices.

As our purpose is to evaluate Eq. (8), it is necessary to explicitly work out the radial and azimuthal components of the velocity field. For the field produced by the point vortices, these components are

$$\begin{aligned} V_r(\mathbf{r}) &= \hat{\mathbf{r}} \cdot \mathbf{v}_v = \frac{1}{r} \frac{\partial \psi_v}{\partial \theta} \\ &= -\sum_n \left(\frac{\Gamma_n}{2\pi} \right) \frac{R_n \sin(\theta - \Theta_n)}{r^2 + R_n^2 - 2rR_n \cos(\theta - \Theta_n)} \end{aligned} \tag{17}$$

and

$$\begin{aligned} V_\theta(\mathbf{r}) &= \hat{\boldsymbol{\theta}} \cdot \mathbf{v}_v = -\frac{\partial \psi_v}{\partial r} \\ &= \sum_n \left(\frac{\Gamma_n}{2\pi} \right) \frac{r - R_n \cos(\theta - \Theta_n)}{r^2 + R_n^2 - 2rR_n \cos(\theta - \Theta_n)}, \end{aligned} \tag{18}$$

where Eqs. (15) and (12) were used to determine $\psi_v(\mathbf{r})$, and the position \mathbf{R}_n of the n th vortex has been written in polar coordinates (R_n, Θ_n) .

It is also necessary to determine the radial and azimuthal components of the velocity field induced by the patch \mathbf{v}_b . This field can be written as a line integral along the contour of the patch using a standard vector identity²⁴

$$\begin{aligned} \mathbf{v}_b &= \nabla \psi_b \times \hat{\mathbf{z}} = \int d\mathbf{r}'^2 \omega_b(\mathbf{r}') \nabla_r G(\mathbf{r} - \mathbf{r}') \times \hat{\mathbf{z}} \\ &= 4\pi \oint d\mathbf{l}' G(\mathbf{r} - \mathbf{r}'), \end{aligned} \tag{19}$$

where $d\mathbf{l}'$ is an infinitesimal vector in the anticlockwise direction along the contour of the vortex patch, and $\mathbf{r}'_c = (r_c(\theta', t), \theta')$ is the point on the contour at angle θ' .

Denoting the $r - \theta$ components of \mathbf{v}_b as u_r and u_θ , respectively, one finds after some algebra²⁶ that Eqs. (19) and (12) yield

$$\begin{aligned} u_r(\mathbf{r}) &= \hat{\mathbf{r}} \cdot \mathbf{v}_b = -2 \int_0^{2\pi} d\theta' \left(\cos(\theta' - \theta) \frac{\partial r'_c}{\partial \theta'} - \sin(\theta' - \theta) r'_c \right) \\ &\quad \times \ln|\mathbf{r}'_c - \mathbf{r}|, \end{aligned} \tag{20}$$

and

$$\begin{aligned} u_\theta(\mathbf{r}) &= \hat{\boldsymbol{\theta}} \cdot \mathbf{v}_b = -2 \int_0^{2\pi} d\theta' \left(\sin(\theta' - \theta) \frac{\partial r'_c}{\partial \theta'} \right. \\ &\quad \left. + \cos(\theta' - \theta) r'_c \right) \ln|\mathbf{r}'_c - \mathbf{r}|. \end{aligned} \tag{21}$$

With the aid of Eqs. (16), (17), (18), (20), and (21) we find that the radial and azimuthal components of the velocity at the contour point \mathbf{r}_c are

$$v_r = V_r(\mathbf{r}_c) + u_r(\mathbf{r}_c), \quad v_\theta = V_\theta(\mathbf{r}_c) + u_\theta(\mathbf{r}_c) - 2\pi r_c, \tag{22}$$

and those at the m th point vortex are

$$\begin{aligned} V_{m,r} &= V'_r(\mathbf{R}_m) + u_r(\mathbf{R}_m), \\ V_{m,\theta} &= V'_\theta(\mathbf{R}_m) + u_\theta(\mathbf{R}_m) - 2\pi R_m, \end{aligned} \tag{23}$$

where $V'_r(\mathbf{R}_m)$ and $V'_\theta(\mathbf{R}_m)$ are given by Eqs. (17) and (18), respectively, with the contribution from the self-field of the

m th point vortex excluded. These expressions for the velocities, together with Eqs. (8) and (9), complete the equations of motion of our model.

B. Perturbation equations

Since our model equations have no general analytic solution, simplifications are necessary in order to proceed. In this section, we Taylor expand the equations of motion in the small parameter λ , the average circulation of the point vortices compared to the circulation of the vortex patch. As we will see later, in order to obtain the leading order solutions that are valid for a time scale of order $1/\lambda$, we need to derive the equation of the contour of the vortex patch correct to $O(\lambda^2)$, and those of the positions of the point vortices to $O(\lambda)$.

The contour of the vortex patch is given by

$$r_c(\theta, t) = 1 + \epsilon(\theta, t), \tag{24}$$

where ϵ is assumed to be a smooth, single valued function of order λ . Since ϵ is a smooth function, $\partial r_c / \partial \theta$ is of order λ ; therefore, in Eq. (8) we need to obtain v_θ to $O(\lambda)$ and v_r to $O(\lambda^2)$. This is accomplished by Taylor expanding the functions $V_r(\mathbf{r}_c), u_r(\mathbf{r}_c)$ and $V_\theta(\mathbf{r}_c), u_\theta(\mathbf{r}_c)$.

Taylor expansion of $V_r(\mathbf{r}_c)$ is straightforward, and using Eq. (17) the result is

$$V_r(\mathbf{r}_c) = \lambda V_r^{(1)}(\theta, t) + \lambda \epsilon(\theta, t) V_r^{(2)}(\theta, t) + O(\lambda^3), \tag{25}$$

where

$$V_r^{(1)}(\theta, t) = - \sum_m \left(\frac{\Gamma_m}{2\pi\lambda} \right) \frac{R_m(t) \sin(\theta - \Theta_m(t))}{1 + R_m(t)^2 - 2R_m(t) \cos(\theta - \Theta_m(t))}, \tag{26}$$

and

$$V_r^{(2)}(\theta, t) = \sum_m \left(\frac{\Gamma_m}{\pi\lambda} \right) \times \frac{R_m(t) \sin(\theta - \Theta_m(t)) (1 - R_m(t) \cos(\theta - \Theta_m(t)))}{(1 + R_m(t)^2 - 2R_m(t) \cos(\theta - \Theta_m(t)))^2}. \tag{27}$$

The function $V_r^{(1)}$ is the radial velocity induced by the point vortices evaluated along the contour of the unperturbed circular patch, and $V_r^{(2)}$ is the correction due to the deformation of the contour from a circle.

Taylor expansion of $u_r(\mathbf{r}_c)$ needs a little more care, since it involves an integration of function $\ln |\mathbf{r}'_c - \mathbf{r}_c|$, which is singular when $\mathbf{r}'_c \rightarrow \mathbf{r}_c$. Nevertheless, one can prove that²⁶

$$u_r(\mathbf{r}_c) = \int_0^{2\pi} d\theta' \left(\epsilon' - \epsilon\epsilon' + \frac{\epsilon'^2}{2} \right) \cot\left(\frac{\theta' - \theta}{2}\right) + O(\lambda^3), \tag{28}$$

where $\epsilon' \equiv \epsilon(\theta, t)$. Combining Eqs. (25) and (28) in Eq. (22) we arrive at the total radial velocity of the contour point

$$v_r(\theta, t) = \lambda V_r^{(1)} + \lambda \epsilon V_r^{(2)} + \int_0^{2\pi} d\theta' \left(\epsilon' - \epsilon\epsilon' + \frac{\epsilon'^2}{2} \right) \cot\left(\frac{\theta' - \theta}{2}\right) + O(\lambda^3). \tag{29}$$

Similarly, the azimuthal velocity components of the patch contour due to the point vortices and the patch itself are found to be

$$V_\theta(r_c) = \lambda V_\theta^{(1)} + O(\lambda^2), \tag{30}$$

where

$$V_\theta^{(1)}(\theta, t) \equiv \sum_m \left(\frac{\Gamma_m}{2\pi\lambda} \right) \times \frac{1 - R_m(t) \cos(\theta - \Theta_m(t))}{1 + R_m(t)^2 - 2R_m(t) \cos(\theta - \Theta_m(t))}, \tag{31}$$

and

$$u_\theta(\mathbf{r}_c) = 2\pi + O(\lambda^2). \tag{32}$$

In Eq. (32) above there is no $O(\lambda)$ term. This is related to the fact that the area of the vortex patch is a constant under incompressible flow, equal to π in our units:

$$\pi = \int_0^{2\pi} d\theta' \int_0^{1+\epsilon'} dr r, \tag{33}$$

which yields

$$\int_0^{2\pi} d\theta' \epsilon' = -\frac{1}{2} \int_0^{2\pi} d\theta' \epsilon'^2 \sim O(\lambda^2). \tag{34}$$

Combining Eqs. (24), (30), and (32), Eq. (22) yields the following expression for the total θ velocity of the patch contour:

$$v_\theta(\theta, t) = -2\pi\epsilon + \lambda V_\theta^{(1)} + O(\lambda^2). \tag{35}$$

Substituting Eqs. (24), (29), and (35) in the evolution equation for the patch contour, Eq. (8), we arrive at

$$\begin{aligned} \frac{\partial \epsilon}{\partial t} + (-2\pi\epsilon + \lambda V_\theta^{(1)}) \frac{\partial \epsilon}{\partial \theta} &= \lambda V_r^{(1)} + \lambda \epsilon V_r^{(2)} \\ &+ \int_0^{2\pi} d\theta' \left(\epsilon' - \epsilon\epsilon' + \frac{\epsilon'^2}{2} \right) \cot\left(\frac{\theta' - \theta}{2}\right), \end{aligned} \tag{36}$$

which is correct to $O(\lambda^2)$.

Turning now to the dynamical equations for the point vortices, according to Eq. (23) we need to Taylor expand $V_{m,r}$ and $V_{m,\theta}$ to $O(\lambda)$. Using Eqs. (20), (21), and (24) in Eq. (23) yields

$$V_{m,r} = V'_r(\mathbf{R}_m) + u'_r(\mathbf{R}_m; \epsilon) + O(\lambda^2), \tag{37}$$

and

$$V_{m,\theta} = V'_\theta(\mathbf{R}_m) + u_\theta^{(1)}(\mathbf{R}_m; \epsilon) + O(\lambda), \quad (38)$$

where

$$u_r^{(1)}(\mathbf{R}_m; \epsilon) = \int_0^{2\pi} d\theta' \frac{2\epsilon(\theta', t) \sin(\theta' - \Theta_m)}{1 + R_m^2 - 2R_m \cos(\theta' - \Theta_m)} \quad (39)$$

and

$$u_\theta^{(1)}(\mathbf{R}_m; \epsilon) = \int_0^{2\pi} d\theta' \frac{2\epsilon(\theta', t)(R_m - \cos(\theta' - \Theta_m))}{1 + R_m^2 - 2R_m \cos(\theta' - \Theta_m)} \quad (40)$$

are the r and θ components of the velocity field due to the patch perturbation ϵ . As an aid to the analysis of Sec. IV the functional dependence of $u_r^{(1)}$ and $u_\theta^{(1)}$ on $\epsilon(\theta', t)$ has been explicitly noted in the second argument of these functions. Therefore, correct to $O(\lambda)$, the perturbation equations for the point vortices are

$$\frac{dR_m}{dt} = V'_r(\mathbf{R}_m) + u_r^{(1)}(\mathbf{R}_m; \epsilon), \quad (41)$$

$$R_m \frac{d\Theta_m}{dt} = V'_\theta(\mathbf{R}_m) + u_\theta^{(1)}(\mathbf{R}_m; \epsilon). \quad (42)$$

Equations (36), (41), and (42) provide a closed set of perturbation equations describing the evolution of the boundary of the vortex patch, and the motions of the point vortices inside the patch, as seen in the rotating frame of the unperturbed patch.

C. Mode equations

The evolution equation for the perturbed patch contour ϵ can be decomposed into the equations for Fourier modes. Let

$$\epsilon(\theta, t) = \sum_k \epsilon_k(t) e^{ik\theta}, \quad (43)$$

where $\epsilon_k(t)$ is the amplitude of the k th mode. Because of the periodic boundary condition $\epsilon(\theta + 2\pi, t) = \epsilon(\theta, t)$, k must be an integer. Moreover, since ϵ is real, we have

$$\epsilon_k^* = \epsilon_{-k}. \quad (44)$$

We also know that

$$\epsilon_0 \sim O(\lambda^2). \quad (45)$$

This is obtained by substituting the Fourier expansion, Eq. (43), into Eq. (34), and is a consequence of the fact that the area of the vortex patch is a conserved quantity.

With Eq. (43), we can obtain the Fourier coefficients of Eq. (36). It is useful to define the following quantities:

$$V_k = \sum_m \frac{\Gamma_m}{4\pi} R_m^{|k|} e^{-ik\Theta_m}, \quad (46)$$

a sum related to the driven response of the contour of the vortex patch due to the point vortices, and a sign function s_k :

$$s_k = \begin{cases} 1, & k > 0 \\ 0, & k = 0 \\ -1, & k < 0 \end{cases}. \quad (47)$$

Then a straightforward but lengthy calculation of the Fourier coefficients of each term in Eq. (36) leads to the following equation for the mode amplitudes of the patch contour:²⁶

$$\begin{aligned} \frac{d\epsilon_k}{dt} = & i2\pi s_k \epsilon_k + i s_k V_k + 2\pi i \sum_q \epsilon_q \epsilon_{k-q} \left(q - s_q + \frac{s_k}{2} \right) \\ & - ik \epsilon_k \sum_m \frac{\Gamma_m}{4\pi} - i \sum_q \epsilon_{k-q} (k + s_q) V_q. \end{aligned} \quad (48)$$

The first term on the right hand side of the above equation represents the restoring force for the oscillation of the k th mode, the second term represents driving by the point vortices, the third term represents mode–mode coupling, and the fourth and the last terms represent nonlinear interactions between modes and the point vortices.

Equation (48) provides the nonlinear evolution of the Kelvin wave amplitude ϵ_k , correct to $O(\lambda^2)$. Note that V_k , defined in Eq. (46), depends on the positions of the point vortices, which must be determined via Eqs. (41) and (42). The nonlinear terms on the right hand side are of order λ^2 except when ϵ_0 , the amplitude of the zeroth mode, is involved, in which case the nonlinear terms are of order λ^3 since $\epsilon_0 \sim O(\lambda^2)$ [Eq. (45)]. Therefore nonlinear terms involving ϵ_0 can be discarded.

IV. SOLUTIONS

A. Kelvin waves

If we set $\Gamma_m = 0$ for all of the point vortices, Eq. (48) becomes the linear mode equation for small disturbances on a circular patch. To the first order in the amplitude of the small disturbances, the equation for the k th mode is

$$\frac{d\epsilon_k}{dt} = i2\pi s_k \epsilon_k, \quad (49)$$

and the solution is

$$\epsilon_k(t) = \epsilon_k(0) e^{2\pi i s_k t}, \quad (50)$$

where $\epsilon_k(0)$ is the initial amplitude of the mode. Therefore, a small disturbance on the circular patch evolves as

$$\epsilon(\theta, t) = \sum_k \epsilon_k(0) e^{i(k\theta + 2\pi s_k t)}, \quad (51)$$

which is a sum of Kelvin waves. The phase velocity of the k th Kelvin wave is

$$v_{\text{phase}} = -\frac{2\pi}{|k|}. \quad (52)$$

In the rotating frame, all Kelvin waves rotate in the clockwise direction. Also notice that all Kelvin waves oscillate with periods equal to unity (normalized to the rotation time of the vortex patch). This means that any arbitrary small disturbance composed of Kelvin waves returns to its initial shape every unit time period, although in between the periods the shape changes due to the different phase velocities of the Kelvin waves.

B. Two time scale analysis

Even in the perturbation limit $\lambda \ll 1$, our model equations are still too complex to solve analytically. Fortunately, further progress is possible by noting that there are two time scales in the dynamics. As shown in Eqs. (41) and (42), the velocity of the m th point vortex in the rotating frame is induced by other point vortices and the small disturbance $\epsilon(\theta, t)$ on the contour of the vortex patch, which are all quantities of order λ . Thus, it takes a slow time scale of order $1/\lambda$ to move the point vortices over distances of order unity relative to the vortex patch. On the other hand, Eq. (50) shows that the modes on the contour of the vortex patch oscillate with a fast time scale of order unity. Therefore we can solve the perturbed equations with two time scale analysis.

We first introduce the ‘‘slow time,’’ defined as $\tau = \lambda t$, and accordingly call t the ‘‘fast time.’’ We then expand the dynamical variables in two time scale series:

$$\epsilon_k(t) = \lambda \epsilon_k^{(1)}(t, \tau) + \lambda^2 \epsilon_k^{(2)}(t, \tau) + \dots, \tag{53}$$

$$R_m(t) = R_m^{(0)}(t, \tau) + \lambda R_m^{(1)}(t, \tau) + \dots, \tag{54}$$

$$\Theta_m(t) = \Theta_m^{(0)}(t, \tau) + \lambda \Theta_m^{(1)}(t, \tau) + \dots, \tag{55}$$

where $\epsilon_k^{(1)}$, $\epsilon_k^{(2)}$, $R_m^{(0)}$, $R_m^{(1)}$, $\Theta_m^{(0)}$, and $\Theta_m^{(1)}$ are functions of order of unity. Here $\epsilon_0^{(1)} = 0$, since ϵ_0 is of order λ^2 [see Eq. (45)].

Substituting these two time scale series into the perturbation equations and collecting terms in the same order of λ , we obtain a series of equations corresponding to the contributions from the terms of successively increasing order in λ . The slow time dependence of a quantity is determined in the next order equations by requiring that the sum of the resonant terms that drive unbounded fast time growth of the next order quantities should vanish (the resonance condition).

For the point vortices, substitution of the two time scale series into Eqs. (41) and (42) yields the $O(\lambda^0)$ equations

$$\frac{\partial R_m^{(0)}}{\partial t} = 0, \quad R_m^{(0)} \frac{\partial \Theta_m^{(0)}}{\partial t} = 0, \tag{56}$$

and the $O(\lambda)$ equations

$$\lambda \left(\frac{\partial R_m^{(0)}}{\partial \tau} + \frac{\partial R_m^{(1)}}{\partial t} \right) = V_r'(\mathbf{R}_m^{(0)}) + u_r^{(1)}(\mathbf{R}_m^{(0)}; \lambda \epsilon^{(1)}), \tag{57}$$

and

$$\begin{aligned} \lambda \left[R_m^{(1)} \frac{\partial \Theta_m^{(0)}}{\partial t} + R_m^{(0)} \left(\frac{\partial \Theta_m^{(0)}}{\partial \tau} + \frac{\partial \Theta_m^{(1)}}{\partial t} \right) \right] \\ = V_\theta'(\mathbf{R}_m^{(0)}) + u_\theta^{(1)}(\mathbf{R}_m^{(0)}; \lambda \epsilon^{(0)}). \end{aligned} \tag{58}$$

Here, V_r' and V_θ' are evaluated with all vortices at their leading-order positions $\mathbf{R}_n^{(0)}$. Equations (57) and (58) involve the lowest-order deformation of the patch contour

$$\lambda \epsilon^{(1)}(\theta, t, \tau) = \lambda \sum_{k \neq 0} \epsilon_k^{(1)}(t, \tau) e^{ik\theta}. \tag{59}$$

This contour evolves according to Eq. (48). Substitution of the two time scale series, Eqs. (53)–(55), gives the $O(\lambda)$ equation

$$\frac{\partial \epsilon_k^{(1)}}{\partial t} = 2\pi i s_k \epsilon_k^{(1)} + i s_k V_k^{(1)}, \tag{60}$$

and the $O(\lambda^2)$ equation

$$\frac{\partial \epsilon_k^{(2)}}{\partial t} - 2\pi i s_k \epsilon_k^{(2)} = h_k, \tag{61}$$

where

$$\begin{aligned} h_k(t, \tau) \equiv & -\frac{\partial \epsilon_k^{(1)}}{\partial \tau} + i s_k V_k^{(2)} + 2\pi i \sum_q \epsilon_q^{(1)} \epsilon_{k-q}^{(1)} \left(q - s_q + \frac{s_k}{2} \right) \\ & - i k \epsilon_k^{(1)} \sum_m \frac{\Gamma_m}{4\pi\lambda} - i \sum_q \epsilon_{k-q}^{(1)} (k + s_q) V_q^{(1)} \end{aligned} \tag{62}$$

is a nonlinear forcing term, and

$$V_k^{(1)} = \sum_m \frac{\Gamma_m}{4\pi\lambda} R_m^{(0)|k|} e^{-ik\Theta_m^{(0)}}, \tag{63}$$

$$V_k^{(2)} = \sum_m \frac{\Gamma_m}{4\pi\lambda} R_m^{(0)|k|} e^{-ik\Theta_m^{(0)}} \left(\frac{|k|R_m^{(1)}}{R_m^{(0)}} - ik\Theta_m^{(1)} \right) \tag{64}$$

constitute the two time series for the quantity V_k [see Eq. (46)]:

$$V_k = \lambda V_k^{(1)} + \lambda^2 V_k^{(2)} + \dots. \tag{65}$$

C. Leading order solutions on the fast time scale

In the leading order, the point vortices move according to Eq. (56). The solution is simply

$$R_m^{(0)} = R_m^{(0)}(\tau), \quad \Theta_m^{(0)} = \Theta_m^{(0)}(\tau), \tag{66}$$

so to leading order the point vortices are stationary in the rotating frame on the fast time scale.

The amplitudes of the modes of the vortex patch evolve in leading order according to Eq. (60). Since $V_k^{(1)}$ only depends on the leading order positions of the point vortices, which have no fast time dependence, the solution of the equation is

$$\epsilon_k^{(1)} = b_k(\tau) e^{2\pi i s_k t} - \frac{V_k^{(1)}}{2\pi}, \tag{67}$$

where $b_k(\tau)$ is the constant of integration that depends on slow time. Therefore,

$$\epsilon^{(1)}(\theta, t, \tau) = \beta(\theta, \tau) + \sum_{k \neq 0} b_k(\tau) e^{2\pi i s_k t}, \tag{68}$$

where

$$\begin{aligned} \beta(\theta, \tau) &= - \sum_{k \neq 0} \frac{V_k^{(1)}}{2\pi} e^{ik\theta} \\ &= \sum_m \left(\frac{\Gamma_m}{4\pi^2\lambda} \right) \frac{R_m^{(0)2} - R_m^{(0)} \cos(\theta - \Theta_m^{(0)})}{1 + R_m^{(0)2} - 2R_m^{(0)} \cos(\theta - \Theta_m^{(0)})}, \end{aligned} \quad (69)$$

where in the second line we have summed the Fourier series, using Eq. (63). Notice that $\lambda\beta(\theta, \tau)$ has the same form as the image charge distribution induced by the point vortices at $\mathbf{R}_m^{(0)}$ on a circular free-slip boundary of radius 1. From Eq. (68) we see that in the leading order, the deformation of the vortex patch consists of two parts: one part is $\beta(\theta, \tau)$, the ‘‘image charge’’ deformation, which is determined by the leading order positions of the point vortices; the other part is free-streaming Kelvin waves with amplitudes $b_k(\tau)$ which are not affected (in fast time) by the point vortices.

D. Leading order solutions on the slow time scale

The slow time evolution of the leading order approximations to the positions of the point vortices $\mathbf{R}_m^{(0)}$ and the contour of the vortex patch $\epsilon^{(1)}(\theta, t, \tau)$ must be determined with the resonant conditions in the next order equations, Eqs. (57), (58), and (61).

Substituting the leading order solutions [Eqs. (66) and (68)] into Eq. (57), we obtain

$$\begin{aligned} \lambda \frac{\partial R_m^{(1)}}{\partial t} &= \left\{ -\lambda \frac{dR_m^{(0)}}{d\tau} + V'_r(\mathbf{R}_m^{(0)}) + u_r^{(1)}(\mathbf{R}_m^{(0)}; \lambda\beta) \right\} \\ &\quad + \lambda \sum_{k \neq 0} 2\pi i s_k b_k(\tau) R_m^{(0)|k|-1} e^{ik\Theta_m^{(0)}} e^{2\pi i s_k t}. \end{aligned} \quad (70)$$

Quantities in the curly bracket in Eq. (70) depend only on the slow time. They must sum to zero; otherwise the solution for $R_m^{(1)}$ will have a term that is linear in t , and will grow unbounded on the fast time scale. Therefore, we have

$$\lambda \frac{dR_m^{(0)}}{d\tau} = V'_r(\mathbf{R}_m^{(0)}) + u_r^{(1)}(\mathbf{R}_m^{(0)}; \lambda\beta) \quad (71)$$

and

$$R_m^{(1)} = \sum_{k \neq 0} b_k(\tau) R_m^{(0)|k|-1} e^{ik\Theta_m^{(0)}} e^{2\pi i s_k t} + c_m(\tau), \quad (72)$$

where $c_m(\tau)$ is a constant of integration.

Similarly for the θ motion of the point vortices, substituting the leading order solutions [Eqs. (66) and (68)] into Eq. (58) implies

$$\lambda R_m^{(0)} \frac{d\Theta_m^{(0)}}{d\tau} = V'_\theta(\mathbf{R}_m^{(0)}) + u_\theta^{(1)}(\mathbf{R}_m^{(0)}; \lambda\beta) \quad (73)$$

and

$$\Theta_m^{(1)} = \sum_{k \neq 0} i s_k b_k(\tau) R_m^{(0)|k|-2} e^{ik\Theta_m^{(0)}} e^{2\pi i s_k t} + d_m(\tau), \quad (74)$$

where $d_m(\tau)$ is a constant of integration.

Equations (71) and (73) show that the leading order positions of the point vortices evolve in the rotating frame on the slow time scale with a velocity induced by other point vortices as well as the image charge part $\lambda\beta$ of the contour deformation of the vortex patch. Therefore, the leading order dynamics of the point vortices is the same as that of point vortices under a circular free-slip boundary with radius equal to that of the vortex patch. Also, Eqs. (72) and (74) show that the free-streaming Kelvin waves excite oscillations of the point vortices on the fast time scale.

To test this conclusion, we have compared the leading order solutions with the results of a contour dynamics simulation²⁴ for the case of $M=2$ and $\Gamma_1 = \Gamma_2 = 0.05 \times 4\pi^2 = 0.2\pi^2$ (i.e., $\lambda=0.05$), initially placed at $\mathbf{R}_1 = (0.2, 0)$ and $\mathbf{R}_2 = (0.4, \pi)$. The evolution of the radial position of the first point vortex is plotted in Fig. 1. As shown in the figure, the leading order solution agrees well with the result of contour dynamics.

The difference between the leading order solution and the result of the contour dynamics is of order $\lambda=0.05$, and has two features that can be understood from the solutions of the $R_m^{(1)}$ and $\Theta_m^{(1)}$, Eqs. (72) and (74). First, there is a fast time scale oscillation with period 1 (the rapid wiggles in the solid line of Fig. 1) that is missing from the leading-order solution (the dashed line). This oscillation comes from the effect of free-streaming Kelvin waves on the vortices; see Eqs. (72) and (74). Second, there is a deviation that evolves on the slow time scale: the slow oscillation frequency in the contour dynamics solution is evidently not quite the same as the leading-order solution. This discrepancy comes from slow-time evolution in the constants of integration $c_m(\tau)$ and $d_m(\tau)$ in Eqs. (72) and (74). The slow time evolution of these small quantities cannot be determined at our order of approximation; they are determined by higher order equations.

The equivalence at lowest nontrivial order of the dynamics of the point vortices to the classical problem of point vortices inside a circular free-slip boundary enables us to apply all of the results of the classical problem to our model. For example, we know the equilibrium patterns of the point vortices and their stability from the works of Havelock,¹⁷ Campbell and Ziff,¹⁸ and others. We also know that the dynamics of the point vortices is Hamiltonian and is chaotic in general.¹⁹

We now turn to the slow time evolution of the vortex patch. The slow time evolution of the image charge part of the contour deformation $\lambda\beta$ is simply determined by the leading order positions of the point vortices, as given by Eq. (69). The slow time evolution of the Kelvin waves, on the other hand, is obtained by the resonant condition of the second order term $\epsilon_k^{(2)}$ in Eq. (61). Since the right hand side of the equation h_k does not depend on $\epsilon_k^{(2)}$, we have

$$\epsilon_k^{(2)} = e^{2\pi i s_k t} \int_0^t dt' h_k(t', \tau) e^{-2\pi i s_k t'} + f_k(\tau) e^{2\pi i s_k t}, \quad (75)$$

where $f_k(\tau)$ is the constant of integration. Furthermore, since the fast time behavior of h_k is determined by $\epsilon^{(1)}$, $R_m^{(1)}$, and

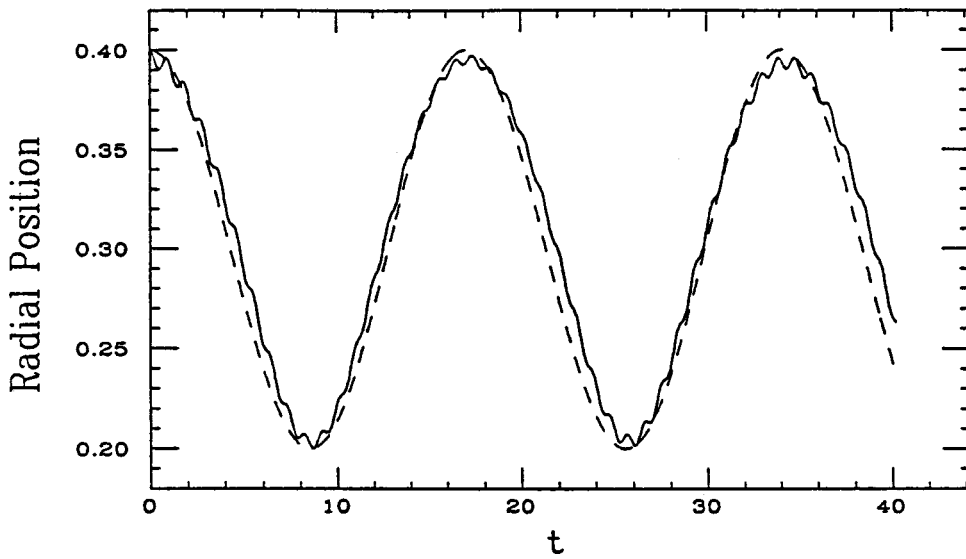


FIG. 1. Time evolution of the radial positions of the first of two point vortices, initially placed at $\mathbf{R}_1=(0.4,\pi)$ and $\mathbf{R}_2=(0.2,0)$. The unit of time is the rotation period of the unperturbed circular patch, and that of the length is the radius of the unperturbed circular patch. The circulations of the point vortices are $\Gamma_1=\Gamma_2=0.2\pi^2$ (i.e., $\lambda=0.05$). The dashed line is the result of the leading order two time scale solutions, Eqs. (71) and (73). The solid line is the result of contour dynamics. The shape of the vortex patch is initially circular. At $t=40.22$, the contour of the vortex patch filaments.

$\Theta_m^{(1)}$, which are all periodic functions of the fast time t within period 1, we can express h_k in terms of the Fourier transformation

$$h_k = \sum_n \hat{h}_k(n, \tau) e^{2\pi i n t}, \tag{76}$$

where the n th Fourier coefficient is defined as

$$\hat{h}_k(n, \tau) = \int_0^1 dt h_k(t, \tau) e^{-2\pi i n t}. \tag{77}$$

Substituting this transformation into Eq. (75), we find that in order to avoid secular growth of $\epsilon_k^{(2)}$ in fast time we require

$$\hat{h}_k(s_k, \tau) = 0, \tag{78}$$

or in other words, the resonant driving term in Eq. (61) must vanish.

Substituting Eqs. (62)–(64) into Eq. (77), and using Eqs. (67), (72), and (74), we find that the above resonant condition leads to the following slow time evolution equations for the amplitudes of the Kelvin waves:

$$\frac{db_k}{d\tau} = ik \sum_{kq>0} W_{k,q} b_q, \tag{79}$$

where the nonlinear coupling matrix $W_{k,q}$ is defined as

$$W_{k,q} = \sum_m \frac{\Gamma_m}{2\pi\lambda} (R_m^{(0)|k|+|q|-2} - R_m^{(0)|k-q|}) e^{i(q-k)\Theta_m^{(0)}}. \tag{80}$$

The details of the derivation are complex and may be found in Ref. 26. Notice that in Eq. (79), only modes with wave numbers of the same sign are coupled. The form of $W_{k,q}$ can be understood by examining the nonlinear terms in h_k [see Eq. (62)]. There are three interactions in the nonlinear terms: interaction between the Kelvin waves and the oscillations of the point vortices, the interaction between the Kelvin waves and the image charge part, and the interaction of the Kelvin waves with other Kelvin waves. The first interaction contributes to the first term in Eq. (80), and the second interaction contributes to the second term in Eq. (80). The third interac-

tion does not contribute, since the sum of the oscillation frequencies of two Kelvin waves does not equal the oscillation frequency of any other Kelvin wave.

A conserved quantity can be derived from the mode equations. From Eq. (80) we see that $W_{k,q}^* = W_{q,k}$. Therefore, it is easy to verify with Eq. (79) that

$$\frac{d}{d\tau} \left(\sum_k \frac{|b_k|^2}{|k|} \right) = \sum_k \left(\frac{b_k^*}{|k|} \frac{db_k}{d\tau} + \frac{b_k}{|k|} \frac{db_k^*}{d\tau} \right) = 0. \tag{81}$$

Hence, the sum $\sum_k |b_k|^2/|k|$ is a conserved quantity. We can prove that this sum multiplied by $8\pi^3\lambda^2$ is the self-energy of the Kelvin waves in the rotating frame (see the Appendix). The conservation of this quantity is not surprising. In the rotating frame, the fast-time averaged energy of the system, which is conserved on the slow time scale, is the sum of the interaction energy between the point vortices, the interaction energy between the point vortices and the image charge part, the self-energy of the image charge part, and the self-energy of the Kelvin waves. On the slow time scale the dynamics of the point vortices in the rotating frame under the influence of the image charge part is the same as if they are subject to a circular free-slip boundary, so the fast-time averaged energy of the subsystem consisting of the point vortices and the image charge part is conserved. Therefore, the fast-time averaged self-energy of the Kelvin waves is also separately conserved.

Equation (79) describes the slow time evolution of the amplitudes of the Kelvin waves. With the image charge part $\lambda\beta$ of the contour deformation slaved by the position of the point vortices, the leading order solution for the contour deformation, Eq. (68), is completely determined. To verify that this solution is indeed correct, we again compare with contour dynamics. In particular, we study the evolution of the contour for the case of $M=1$, $\Gamma_1=0.05 \times 4\pi^2=0.2\pi^2$ (i.e., $\lambda=0.05$). Initially, the point vortex is placed at $\mathbf{R}=(0.5,0)$, and the initial shape of the contour is circular. The leading order motion of the point vortex is quite simple, since the point vortex is moving in the rotating frame only under the influence of its own image charge. The radial po-

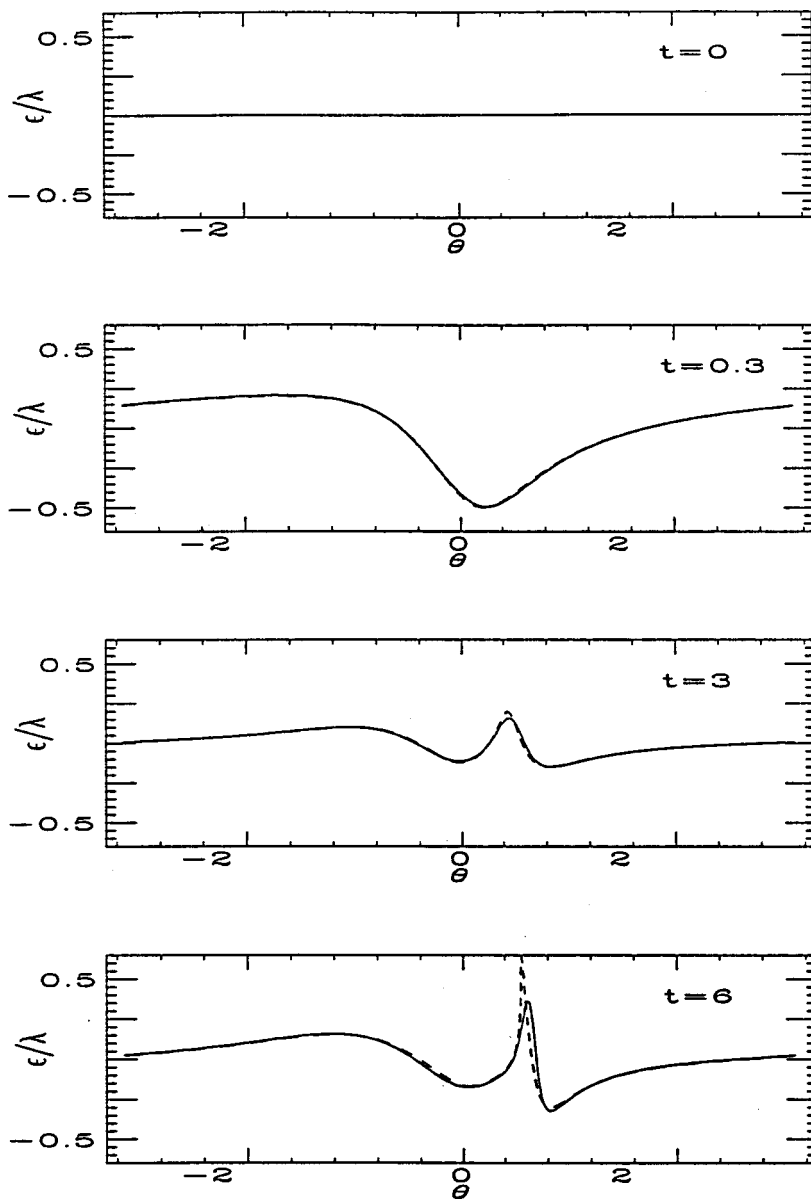


FIG. 2. The evolution of the contour of the vortex patch for the case of one point vortex with circulation $\Gamma_1 = 0.2\pi^2$ (i.e., $\lambda = 0.05$) placed at $(r, \theta) = (0.5, 0)$. The deviation ϵ from the initial circular shape is plotted at $t = 0, 0.3, 3,$ and 6 . The dashed lines are the results of contour dynamics. The solid lines are the results of the mode equations with $-80 \leq k \leq 80$.

sition R of the point vortex does not change, but its angular position increases in slow time as $\Theta = \Omega \tau$, where

$$\Omega = \frac{2}{1 - R^2}. \tag{82}$$

With the position of the point vortex known, the image charge part β is determined by Eq. (69). The evolution of the Kelvin waves is then calculated by evaluating the mode amplitudes, Eqs. (79), up to $k = \pm 80$. We plot the resulting contour deformation in the rotating frame in which the point vortex is stationary in the leading order approximation. The comparison with the result of contour dynamics is quite good at early times, as shown in Fig. 2. However, at late times the contour of the vortex patch steepens and the approximations used in our analysis break down. This is discussed in detail in the next section.

E. Filamentation

For some initial positions of the point vortices, the contour of the vortex patch evolves into a shape that violates the assumptions of the perturbation limit, as seen in Fig. 2. Subsequently, strong nonlinearity takes over and the contour filaments, leading to the breakdown of the leading order solutions. Depending on the positions of the point vortices, filamentation can take place on fast or slow time scales.

The fast time scale filamentation happens when some of the point vortices are very close to the boundary of the vortex patch. In this case, the image charge part of the contour deformation $\lambda\beta(\theta, \tau)$ can be very large. We can estimate the maximum of $|\lambda\beta|$ from the contribution of the point vortex that is closest to the boundary of the vortex patch. If Γ_m and $(R_m^{(0)}, \Theta_m^{(0)})$ are its circulation and leading order position, respectively, then the contribution to $\lambda\beta$ is

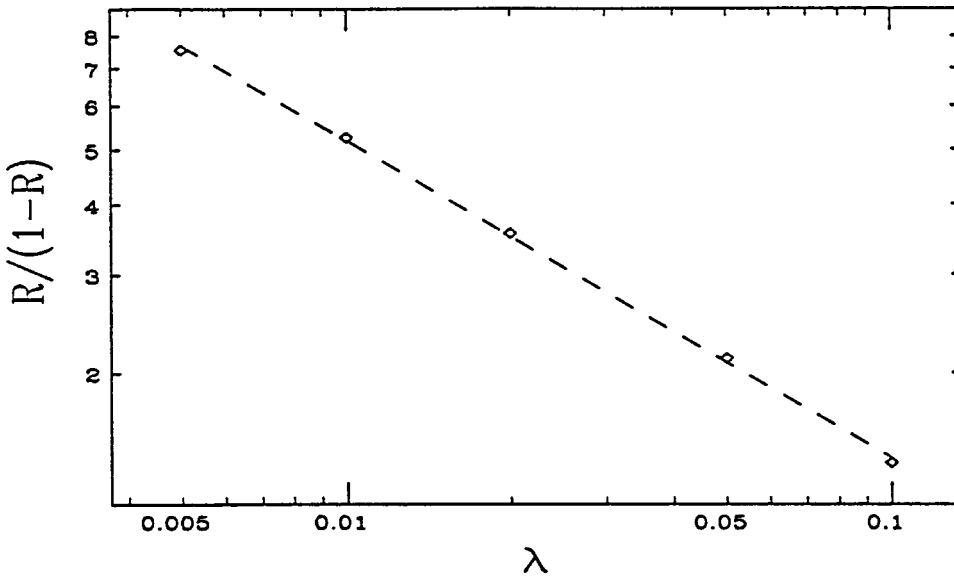


FIG. 3. Fast time point vortex strength filamentation: the relation between λ and $R/(1-R)$, where R is the radial position of a single point vortex for which an initially circular contour filaments at time $t = 1 \pm 0.02$. The dashed line, which has a slope -0.566 , is the best fit to the data.

$$\frac{\Gamma_m(R_m^{(0)2} - R_m^{(0)} \cos(\theta - \Theta_m^{(0)}))}{4\pi^2(1 + R_m^{(0)2} - 2R_m^{(0)} \cos(\theta - \Theta_m^{(0)}))} \quad (83)$$

[see Eq. (69)]. The maximum of the absolute value of the above quantity is

$$\frac{\Gamma_m R_m^{(0)}}{4\pi^2(1 - R_m^{(0)})}. \quad (84)$$

Therefore, if

$$R_m^{(0)} \sim 1 - \lambda^\xi, \quad (85)$$

where $\xi > 0$ is a constant, then the maximum of $\lambda\beta$ is of order $\lambda^{1-\xi} \gg \lambda$ since $\lambda \ll 1$. In this case, the contour deformation, which is the sum of the Kelvin waves and the image charge part, will develop a maximum deformation of order $\lambda^{1-\xi}$ within one rotation time of the vortex patch, although initially the deformation is of order λ . As a consequence, the assumption of the perturbation limit will break down within one rotation time of the vortex patch, leading to fast time scale filamentation of the contour. Equation (85) is the criterion for onset of fast time scale filamentation.

We can estimate the value of the constant ξ with contour dynamics simulations for the simple case of one point vortex placed in a initially circular vortex patch. For a given circulation $\Gamma_1 = 4\pi^2\lambda$, the position of the point vortex R_1 , for which the contour of the vortex patch filaments at $t = 1 \pm 0.02$, is obtained. From several values of λ and the corresponding values of R_1 , we find that $\xi \approx 0.566$, as shown in Fig. 3.

If none of the point vortices is close enough to the edge of the vortex patch, the contour does not filament on the fast time scale. However, it can still filament on a slow time scale. To investigate this possibility, we study the evolution of the ‘‘envelope’’ of the Kelvin waves, defined as

$$\chi(\theta, \tau) = \sum_{k \neq 0} b_k(\tau) e^{ik\theta}. \quad (86)$$

The evolution of this envelope function is determined by the mode equations of the Kelvin waves, Eq. (79).

The filamentation of the Kelvin waves on the slow time scale is tied to the development of a singularity in the envelope function from a smooth initial condition. Since $\sum_k |b_k|^2 / |k|$ is conserved, mode amplitudes of the Kelvin waves cannot become unbounded; therefore, the only way to develop a singularity in $\chi(\theta, \tau)$ is to excite high k modes and form a large gradient.

We argue that the nature of the singularity formation in χ is the same as that in the ‘‘pseudoenvelope’’ $\chi'(\theta, \tau)$, which evolves according to the following simple differential equation:

$$\frac{\partial \chi'}{\partial \tau} + 2 \left(U(\theta, \tau) - \sum_m \frac{\Gamma_m}{4\pi\lambda} \right) \frac{\partial \chi'}{\partial \theta} = 0, \quad (87)$$

where U is obtained from Eq. (30) by replacing the positions of the point vortices with their leading order values, i.e.,

$$U(\theta, \tau) = \sum_m \frac{\Gamma_m(1 - R_m^{(0)} \cos(\theta - \Theta_m^{(0)}))}{2\pi\lambda(1 + R_m^{(0)2} - 2R_m^{(0)} \cos(\theta - \Theta_m^{(0)}))}. \quad (88)$$

The pseudoenvelope can be decomposed into Fourier modes:

$$\chi'(\theta, \tau) = \sum_k b'_k(\tau) e^{ik\theta}, \quad (89)$$

where b'_k is the amplitude of the k th mode. From Eq. (87) we obtain

$$\frac{db'_k}{d\tau} = i \sum_q W'_{k,q} b'_q, \quad (90)$$

where

$$W'_{k,q} = - \sum_m q \frac{\Gamma_m}{2\pi\lambda} R_m^{(0)|k-q|} e^{i(q-k)\Theta_m^{(0)}}. \quad (91)$$

The mode equations (90) are different from the mode equations (79), therefore, the details of the pseudoenvelope χ' are

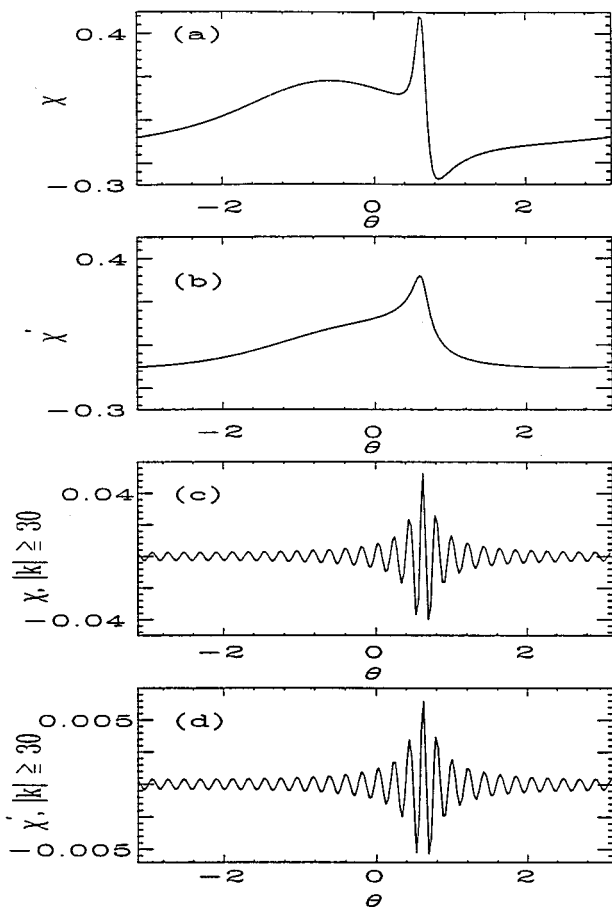


FIG. 4. Comparison of the envelope of Kelvin waves, $\chi(\theta, t)$, and the pseudoenvelope, $\chi'(\theta, t)$, at $t=6$ for the case of one point vortex with $\Gamma_1 = 0.2\pi^2$ (i.e., $\lambda = 0.05$) placed at $(r, \theta) = (0.5, 0)$. Initially the vortex patch is circular. Mode equations with $-80 \leq k \leq 80$ are integrated. (a) χ ; (b) χ' ; (c) part of χ that only include contributions from modes with $|k| \geq 30$; (d) part of χ' that only include contributions from modes with $|k| \geq 30$.

different from the envelope χ for the Kelvin waves. However, for $|k| \geq 1$, since $R_m^{(0)} < 1$, Eqs. (91) and (80) imply

$$W'_{k,q} \approx \begin{cases} kW_{k,q}, & kq > 0 \\ 0, & kq < 0 \end{cases} \quad (92)$$

Furthermore, in both cases modes are coupled most effectively only to nearby modes, i.e., $|q - k|$ must be small. Thus, the high $|k|$ modes are not effectively coupled to the low $|k|$ modes, which presumably behave quite differently for χ' and χ since $W'_{k,q}$ are quite different from $kW_{k,q}$ for small $|k|$. Therefore, high $|k|$ modes are excited in the same way in both χ and χ' , and we can hope to understand the development of the singularity in χ by studying the behavior of χ' , which is much simpler.

To illustrate these points, we numerically integrate the mode equations for χ , Eq. (79), and the mode equations for χ' , Eq. (90). The calculation is again for the case of one point vortex with $\Gamma_1 = 0.05 \times 4\pi^2 = 0.2\pi^2$ placed at $\mathbf{R}_1 = (0.5, 0)$ in an initially circular vortex patch. We plot in Figs. 4(a) and 4(b) χ and χ' at $t=6$, right before the contour filaments, in the rotating frame in which the point vortex is stationary. As can be seen in the figures, the overall shapes of χ and χ' are different. However, there are similarities

which can be most easily observed if we plot only the high k mode contributions to χ and χ' . In Figs. 4(c) and 4(d), we plot the parts of χ and χ' that include only modes with $|k| \geq 30$. Although the absolute magnitudes are different, the two curves are very similar in shape, indicating that the pseudoenvelope equation has captured the important high- k coupling responsible for filamentation.

Equation (87) is amenable to the method of characteristics. Defining characteristics according to

$$\frac{d\theta}{d\tau} = 2 \left(U(\theta, \tau) - \sum_m \frac{\Gamma_m}{4\pi\lambda} \right), \quad (93)$$

Eq. (87) becomes $d\chi'(\theta(\tau), \tau)/d\tau = 0$. We observe from this equation that the value of χ' on a pseudoenvelope point remains constant for all time. Therefore, the singularity can form only if the pseudoenvelope points converge within arbitrarily small distances, which makes the gradient of the pseudoenvelope with respect to the angle very large. If the angular distance $\delta\theta(\tau)$ between two pseudoenvelope points, originally separated by a distance $\delta\theta_0$ of order unity, come close to each other within a distance of order $\delta\theta_0\lambda^\eta$, where $\eta > 0$ is a constant, then the gradient of the pseudoenvelope will be amplified by a factor of order $\lambda/\lambda^\eta = \lambda^{1-\eta} \gg \lambda$ since $\lambda \ll 1$. At this point, the pseudoenvelope is not smooth, and a singularity forms. Equation (93) shows that the angular position of a point on the pseudoenvelope evolves according to a first order differential equation in slow time. This implies that when two points on the pseudoenvelope converge, their angular distance can only decrease exponentially in slow time. We will soon see that such exponential convergence of boundary points is associated with an attractive fixed point in the θ dynamics of the pseudoenvelope. Therefore, the time τ_B at which the singularity forms on the pseudoenvelope can be estimated as follows:

$$\delta\theta(\tau) \approx \delta\theta_0 e^{-\gamma\tau_B} \approx \delta\theta_0 \lambda^\eta, \quad (94)$$

or equivalently,

$$t_B \equiv \frac{\tau_B}{\lambda} \approx \frac{\eta}{\gamma} \lambda^{-1} \ln \lambda^{-1}. \quad (95)$$

Here γ is a constant, determined from the characteristics of Eq. (93) and depending on the dynamics of the point vortices.

Since the nature of singularity formation in χ is the same as that in χ' , t_B is also the time at which the singularity forms in χ . At this point, our perturbation solution for the Kelvin waves breaks down, and strong nonlinearity takes over. We can assume that filamentation follows very quickly after this point, since the gradient is already high, and strong nonlinear interaction occurs. Therefore, t_B is also the filamentation time for the Kelvin waves in our model.

The constant η is an exponent that measures the strength of nonlinearity needed for the breakdown of the perturbation equations. Since its role is similar to that of the exponent ξ that we previously determined for the case of fast time scale filamentation [see the discussion that follows Eq. (85)], we assume that $\eta \approx \xi = 0.566$. Note that the precise value of η is not important for the scaling of t_B with λ .

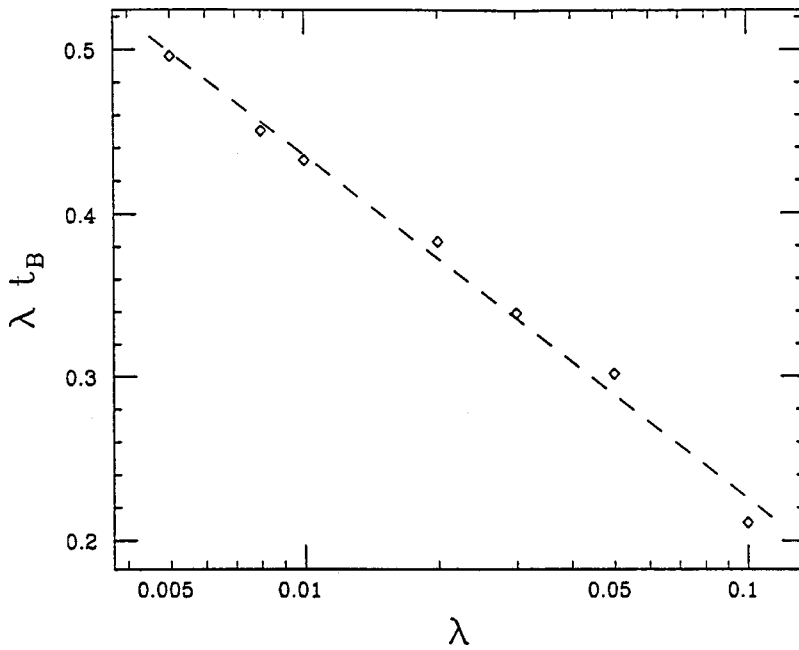


FIG. 5. The dependence of the filamentation time t_B on point vortex strength λ . Initially, the point vortex is at $(r, \theta) = (0.5, 0)$, and the contour of the vortex patch is circular. The dashed line, which is for visual aid, has a slope -1 .

To show that the above approach is useful for understanding the slow time scale filamentation of the Kelvin waves, we present two simple examples. In both examples, we study the formation of singularity in the pseudoenvelopes, and infer from the results the nature of filamentation of the Kelvin waves.

The first example is the case of one point vortex with circulation $\Gamma_1 = 4\pi^2\lambda$ placed at radial position R . The leading order solution of the point vortex is very simple, as we have shown in the previous section: the radial position of the point vortex does not change, and its angular position is given by Eq. (82). With the motion of the point vortex known, the equation for the points on the pseudoenvelope, Eq. (93), becomes

$$\frac{d\theta'}{d\tau} = \frac{2(1-R^2)}{1+R^2-2R\cos(\theta')} + \Omega, \tag{96}$$

where $\theta' \equiv \theta - \Omega\tau$, indicating that Eq. (96) is written in a rotating frame, chosen so that the point vortex is stationary [see Eq. (82)]. The fixed points θ'_{fix} of Eq. (96) are given by $d\theta'/d\tau = 0$, and the solution is

$$\cos(\theta'_{\text{fix}}) = \frac{R(3-R^2)}{2}. \tag{97}$$

It is easy to see that for all $0 < R < 1$, the right hand side of the above equation is always positive and smaller than 1. Therefore, the equation always has two fixed points, one is between 0 and $\pi/2$, the other is between $3\pi/2$ and 2π . To see the behavior of the pseudoenvelope points nearby the fixed points, we Taylor expand the right hand side of Eq. (96) near the fixed point and get

$$\frac{d(\theta' - \theta'_{\text{fix}})}{d\tau} = -\gamma(\theta' - \theta'_{\text{fix}}), \tag{98}$$

where

$$\gamma = \frac{4R \sin(\theta'_{\text{fix}})}{(1-R^2)^3}. \tag{99}$$

Therefore,

$$\theta'(\tau) - \theta'_{\text{fix}} = (\theta'_0 - \theta'_{\text{fix}}) e^{-\gamma\tau}, \tag{100}$$

where θ'_0 is the initial position of the boundary point. For the fixed point between 0 and $\pi/2$, Eq. (99) shows that $\gamma > 0$; therefore, the boundary points nearby will converge to this fixed point exponentially in time. This fixed point is the stable fixed point. For the other fixed point, which is between $3\pi/2$ and 2π , Eq. (99) shows that $\gamma < 0$; therefore, this fixed point is unstable.

These results indicate that for the case of one point vortex placed off the center of the vortex patch, there is always one boundary point to which the other boundary points converge in slow time. Therefore, the perturbation solutions always break down in finite time t_B . We can estimate t_B using Eqs. (95), (99), and (97):

$$t_B \approx \frac{\eta}{\gamma} \lambda^{-1} \ln \lambda^{-1} = \frac{\eta(1-R^2)^2}{2R\sqrt{4-R^2}} \lambda^{-1} \ln \lambda^{-1}. \tag{101}$$

From the equation above we see that when R is small it takes a long time to filament the Kelvin waves; on the other hand, when R approaches 1, i.e., the point vortex approaches the boundary of the vortex patch, the filamentation time is small. However, Eq. (101) is only valid provided that $t_B \gg 1$; otherwise fast time filamentation sets in.

We have tested Eq. (101), which is inferred from the singularity formation in the pseudoenvelope, with contour dynamics simulations. In the simulations, a point vortex is placed at R and the initial shape of the vortex patch is circular. In Fig. 5, we plot the dependence of the filamentation time in the simulations with $R=0.5$ on λ . The figure shows that the $\lambda^{-1} \ln \lambda^{-1}$ scaling of t_B in Eq. (101) is well satisfied.

In Fig. 6, we plot the dependence of the filamentation time in the simulations with $\lambda = 0.05$ (i.e., the circulation of the point vortex is $\Gamma_1 = 0.2\pi^2$) on the position R of the point vortex. The figure shows that Eq. (101) agrees qualitatively with the results of the contour dynamics.

The second example is the case of two point vortices, with circulations $\Gamma_1 = \Gamma_2 = 4\pi^2\lambda$, initially placed at $(R, 0)$ and (R, π) . Evaluating Eqs. (71) and (73) for this case, we find that the leading order solution of the positions of the point vortices are given by

$$R_1^{(0)} = R = R_2^{(0)}, \tag{102}$$

$$\Theta_1^{(0)} = \Omega\tau, \quad \Theta_2^{(0)} = \pi + \Omega\tau, \tag{103}$$

where

$$\Omega \approx \frac{1 + 3R^4}{R^2(1 - R^4)}. \tag{104}$$

In other words, the point vortices are in equilibrium in the rotating frame with angular frequency $2\pi + \lambda\Omega$. Therefore, the equation of motion for the envelope points, Eq. (93), becomes

$$\frac{d\theta'}{d\tau} = -\Omega + \frac{4(1 - R^4)}{(1 + R^2)^2 - 4R^2 \cos^2(\theta')}, \tag{105}$$

where $\theta' = \theta - \Omega\tau$. The fixed point of the above equation is given by

$$\cos^2(\theta'_{\text{fix}}) = \frac{(1 + R^2)^2}{4R^2} - \frac{(1 - R^4)^2}{1 + 3R^4}. \tag{106}$$

For $1 > R > R_c = 0.44$, there are four solutions for θ'_{fix} , two of which are stable fixed points. As in the previous example, Taylor expansion of the right hand side of Eq. (105) near the stable fixed points reveals exponential convergence of the pseudoenvelope points to the fixed points with

$$\gamma = \frac{16R^2(1 - R^4)\sin(2\theta'_{\text{fix}})}{[(1 + R^2)^2 - 4R^2 \cos^2(2\theta'_{\text{fix}})]^2}. \tag{107}$$

Because of symmetry, γ is the same for the two stable fixed points. As in the previous example, the pseudoenvelope develops singularity at time t_B , which can be inferred as the time at which the Kelvin waves filament. We can estimate t_B using Eqs. (95), (107), and (106):

$$t_B \approx \frac{\eta}{\gamma} \lambda^{-1} \ln \lambda^{-1} = \frac{2\eta(1 - R^4)^2 R^4 \lambda^{-1} \ln \lambda^{-1}}{(1 + 3R^4) \sqrt{(-1 + 4R^2 + 5R^4 + 4R^6)(1 - 4R^2 + 11R^4 - 4R^6)}}. \tag{108}$$

For $R < R_c = 0.44$, there is no solution for θ'_{fix} and, therefore, there is no fixed point for the pseudoenvelope points to converge to. This suggests that the slow time scale filamentation of the Kelvin waves is suppressed for $R < R_c$.

Contour dynamics is again used to verify these results. In Fig. 7 we have plotted the results of contour dynamics for the dependence of the filamentation time, scaled by a factor

of $\lambda^{-1} \ln \lambda^{-1}$, on R for several λ . The initial shape of the contour is circular. As we can see, the $\lambda^{-1} \ln \lambda^{-1}$ scaling of t_B , suggested by Eq. (108), works quite well for $R < 0.7$, as indicated by the coincidence of the scaled filamentation times for different values of λ . For $R > 0.7$, the scaling does not work well for relatively large λ . This is because as R goes close to the edge of the vortex patch, the fast time

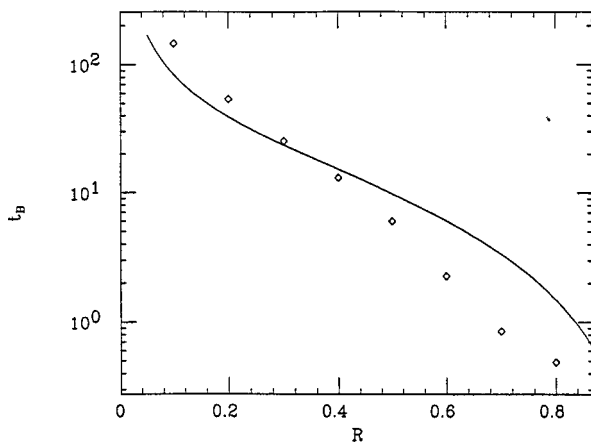


FIG. 6. The dependence of the filamentation time t_B on the position R of the point vortex. The point vortex has a circulation $\Gamma_1 = 0.05 \times 4\pi^2 = 0.2\pi^2$, and is placed initially at $(r, \theta) = (R, 0)$ in a circular vortex patch. The symbol (\diamond) indicates the results of the contour dynamics simulation, and the solid line is the prediction inferred from the evolution of the pseudoenvelope, Eq. (101).

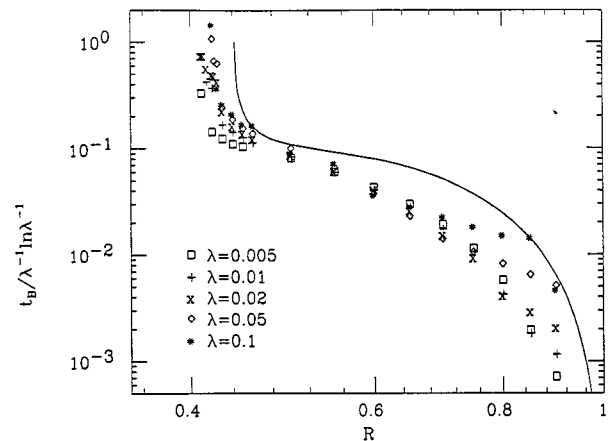


FIG. 7. Dependence of filamentation time t_B on R for the case of two point vortices with equal circulations $4\pi^2\lambda$ initially placed at $(r, \theta) = (R, 0)$ and $(r, \theta) = (R, \pi)$. The shape of the vortex patch is initially circular. The data for five values of λ are presented by the symbols, with t_B scaled by $\lambda^{-1} \ln \lambda^{-1}$. The solid line is the prediction inferred from the evolution of the pseudoenvelope, Eq. (108), scaled by $\lambda^{-1} \ln \lambda^{-1}$.

filamentation, as discussed in the beginning of this section, takes over and the Kelvin waves filament within one rotation of the vortex patch. For $R < R_c$, the filamentation times increase dramatically as R decreases, indicating the suppression of the slow time filamentation for small R . The dependence of t_B on R agrees qualitatively with the formula given by Eq. (108), as in the first example.

The two examples we have discussed above show that dynamics of the slow time filamentation of the Kelvin waves can be understood from the singularity formation in the pseudoenvelope χ' . These examples confirm that the filamentation of the Kelvin waves happens due to the excitation of high k modes, and the filamentation time t_B scales with λ as shown in Eq. (95). They also show that dependence of t_B on the dynamics of the point vortices can be qualitatively deduced from the dynamics of χ' .

The use of the pseudoenvelope greatly simplifies the study of the slow time scale filamentation of the Kelvin waves. However, when the point vortices are in generic positions, the analysis of the slow time filamentation of the Kelvin waves becomes quite complicated since the dynamics of the point vortices are chaotic in most cases. So far, we have not been able to work out the conditions for slow time filamentation for the most general initial positions of the point vortices. Contour dynamics simulations seem to suggest that the slow time filamentation of the Kelvin waves in the most general cases resembles that of a single point vortex placed at the center of charge of the point vortices, off the center of the vortex patch, as studied in the first example. Also, the suppression of the slow time filamentation when the point vortices are clustered near the center of the vortex patch, as studied in the second example, seems to hold in general. These numerical results should be investigated more fully in future studies.

V. DISCUSSION

In this paper, we have studied the dynamics of point vortices inside a nearly circular vortex patch. We first derived general nonlinear equations of motion for the point vorticities and the contour of the vortex patch. Next, we Taylor expanded these equations in powers of the point vortex strength λ , defined as the ratio of the average circulation of the point vortices to the circulation of the patch. We then performed a two time scale analysis of the resulting nonlinear dynamics. The fast scale was determined by the frequency of Kelvin waves on the patch, and the slow time scale was determined by the slow motion of the point vortices in their mutual velocity fields as well as the field of the patch. We showed that in the rotating frame of the vortex patch, the slow time dynamics of the point vortices is equivalent to that of point vortices inside a circular free-slip boundary. The Kelvin waves on the vortex patch cause the point vortices to oscillate on the fast time scale around their slow time scale trajectory.

We also showed that the Kelvin waves break in finite time due to the nonlinear interaction between the point vortices and the vortex patch. When the point vortices are close to the edge of the patch, the filamentation occurs rapidly,

within one rotation period of the patch. This fast filamentation was found to occur when a vortex is on the order of λ^ξ from the patch edge, with $\xi \approx 0.566$ determined from contour dynamics simulations.

On the other hand, when the vortices are far from the patch edge, filamentation occurs on the slow time scale. Using an analysis based on a novel pseudoenvelope formulation of the slow-time nonlinear dynamics of the patch, we found that filamentation occurs when perturbations on the patch steepen as they are attracted to fixed points whose locations are determined by the point vortex positions. The time required for filamentation was shown to scale as $\lambda^{-1} \ln \lambda^{-1}$. This scaling has been verified in recent experiments.²⁵

We then studied the slow filamentation time scale in more detail for two cases: a single point vortex, and two point vortices in equilibrium positions. For the first case, we found that the slow time scale filamentation of the vortex patch always occurs, with the expected time scale, given by Eq. (101). For the latter case, we found that the filamentation can only happen when the radial position of the point vortices is greater than $R_c = 0.44$, with a time scale given by Eq. (108). Contour dynamics simulations suggest that in the general case of many point vortices moving chaotically, the filamentation of the vortex patch resembles the case of one point vortex. In future work, this should be investigated in more detail with both theory and simulations.

In this paper the patch was given a uniform vorticity. However, in any real system the vorticity must fall smoothly to zero at large distances from the center of the patch. This could cause spatial Landau damping of the Kelvin waves, which may suppress filamentation. The influence of spatial variation in the background on the dynamics will be the subject of future work.

Finally, a few words about late-time behavior of the system. Our analysis breaks down after the patch filaments. The complex nonlinear processes responsible for subsequent mixing and stretching of the filamentary structures, and the effect of this mixing on the motion of the point vortices, are beyond the scope of this paper. However, preliminary work using vortex-in-cell simulations indicates that the filamentation eventually leads to chaotic and irreversible mixing of the entire vortex patch as the edge contour is mixed into the interior of the patch,²⁶ and that this mixing can occur even for the simplest possible case of a single point vortex inside the patch. Thus, this relatively simple system displays many of the features of more complex physical systems that involve interactions between vortices and extended vorticity regions, such as atmospheric cyclones interacting with zonal flows, eddies interacting with oceanic currents, vortex crystal experiments, etc. It is hoped that future work on the chaotic dynamics of this simple point vortex/patch system will provide more useful insights into the complex interplay between strong vortices and a background vorticity region.²⁷

ACKNOWLEDGMENTS

This work was supported by NSF Grant No. PHY-9876999 and ONR Grant No. N0.N00014-96-1-0239.

APPENDIX

Here we outline the proof that the sum $8\pi^3\lambda^2\sum_k|b_k|^2/|k|$ is the self-energy of the Kelvin waves in the rotating frame. We first derive an expression for the angular momentum L of the patch:

$$\begin{aligned} L &= -\frac{1}{2}\int_0^{2\pi}d\theta\int_0^{1+\epsilon}dr4\pi r^3 \\ &= -\pi^2-2\pi\int_0^{2\pi}d\theta\epsilon-3\pi\int_0^{2\pi}d\theta\epsilon^2+O(\lambda^3) \\ &= L_0-2\pi\int_0^{2\pi}d\theta\epsilon^2+O(\lambda^3), \end{aligned} \tag{A1}$$

where in the third line we have used Eq. (34), and where $L_0=-\pi^2$ is the angular momentum of the unperturbed patch. Replacing ϵ by its Fourier series, Eq. (43), the angular momentum $L_\epsilon=L-L_0$ due to the contour deformation is found to be

$$L_\epsilon=-4\pi^2\sum_{k\neq 0}|\epsilon_k|^2 \tag{A2}$$

correct to $O(\lambda^2)$.

We now turn to the self-energy of the patch as viewed in the laboratory frame:

$$\begin{aligned} H &= -2\pi\int_0^{2\pi}d\theta\int_0^{2\pi}d\theta'\int_0^{1+\epsilon}rdr\int_0^{1+\epsilon'}dr'r' \\ &\quad \cdot \ln(r^2+r'^2-2rr'\cos(\theta-\theta')), \end{aligned} \tag{A3}$$

where the Green's function, Eq. (12), has been employed. These integrals can be evaluated analytically by Taylor expanding to $O(\lambda^2)$; details may be found in Ref. 26. The result is

$$\begin{aligned} H &= H_0-4\pi^2\int_0^{2\pi}\epsilon^2-2\pi\int_0^{2\pi}\epsilon d\theta\int_0^{2\pi}\epsilon' d\theta' \\ &\quad \times \ln(2-2\cos(\theta-\theta'))+O(\lambda^2) \\ &= H_0-8\pi^3\sum_{k\neq 0}\left(1-\frac{1}{|k|}\right)|\epsilon_k|^2+O(\lambda^3), \end{aligned} \tag{A4}$$

where $H_0=\pi^3$ is the energy of the unperturbed patch, and in the second line we have substituted the Fourier series for ϵ , Eq. (43).

Next, we define the perturbed self-energy $H_\epsilon=H-H_0$ due to the contour deformation. Going to the rotating frame (rotating with angular frequency 2π) the self-energy transforms to

$$H_\epsilon-2\pi L_\epsilon=8\pi^3\sum_{k\neq 0}\frac{|\epsilon_k|^2}{|k|}, \tag{A5}$$

correct to $O(\lambda^2)$. Substituting Eqs. (53) and (67), we obtain the fast-time averaged self-energy of the contour distortion

$$\langle H_\epsilon-2\pi L_\epsilon \rangle=8\pi^3\lambda^2\sum_{k\neq 0}\frac{|b_k|^2}{|k|}+8\pi^3\lambda^2\sum_{\neq 0}\frac{|V_k^{(1)}|^2}{4\pi^2|k|}. \tag{A6}$$

In Eq. (A6), the first term is the self-energy of the Kelvin waves; the second term is that of the image charge.

¹D. G. Dritschel and B. Legras, "Modeling oceanic and atmospheric vortices," *Phys. Today* **46**(3), 44 (1993).
²U. Frisch, *Turbulence* (Cambridge University Press, Cambridge, 1995), p. 240.
³P. S. Marcus, "Numerical simulation of Jupiter's Great Red Spot," *Nature* (London) **331**, 693 (1988).
⁴J. Sommeria, S. P. Meyers, and H. L. Swinney, "Laboratory simulation of Jupiter's Great Red Spot," *Nature* (London) **331**, 689 (1988).
⁵A. P. Ingersoll, "Atmospheric dynamics of the outer planets," *Science* **248**, 308 (1990).
⁶M. R. Brown, "Experimental evidence of rapid relaxation to large-scale structures in turbulent fluids: Selective decay and maximal entropy," *J. Plasma Phys.* **57**, 203 (1997).
⁷C. F. Driscoll and K. S. Fine, "Experiments on vortex dynamics in pure electron plasma," *Phys. Fluids B* **2**, 1359 (1990).
⁸P. Tabeling, S. Burkhart, O. Cardoso, and H. Willaime, "Experimental study of freely decaying two-dimensional turbulence," *Phys. Rev. Lett.* **67**, 3772 (1991).
⁹B. K. Martin, X. L. Wu, W. I. Goldburg, and M. A. Rutgers, "Spectra of decaying turbulence in a soap film," *Phys. Rev. Lett.* **80**, 3964 (1998).
¹⁰J. C. McWilliams, "The emergence of isolated coherent vortices in turbulent flow," *J. Fluid Mech.* **146**, 21 (1984).
¹¹R. Benzi, S. Patarnello, and P. Santangelo, "On the statistical properties of two-dimensional decaying turbulence," *Europhys. Lett.* **3**, 811 (1987).
¹²K. S. Fine, A. C. Cass, W. G. Flynn, and C. F. Driscoll, "Relaxation of 2D turbulence to vortex crystals," *Phys. Rev. Lett.* **75**, 3277 (1995).
¹³D. A. Schecter and D. H. E. Dubin, "Vortex motion driven by a background vorticity gradient," *Phys. Rev. Lett.* **83**, 2191 (1999).
¹⁴D. Z. Jin and D. H. E. Dubin, "Regional maximum entropy theory of vortex crystal formation," *Phys. Rev. Lett.* **80**, 4434 (1998).
¹⁵D. Z. Jin and D. H. E. Dubin, "Characteristics of two-dimensional turbulence that self-organizes into vortex crystals," *Phys. Rev. Lett.* **84**, 1443 (2000).
¹⁶I. M. Lanksy, T. M. O'Neil, and D. A. Schecter, "A theory of vortex merger," *Phys. Rev. Lett.* **79**, 1479 (1997).
¹⁷T. H. Havelock, "The stability of motion of rectilinear vortices in ring formation," *Philos. Mag.* **11**, 617 (1931).
¹⁸L. J. Campbell and R. M. Ziff, "Vortex patterns and energies in a rotating superfluid," *Phys. Rev. B* **20**, 1886 (1979).
¹⁹H. Aref, "Integrable, chaotic, and turbulent vortex motion in two-dimensional flows," *Annu. Rev. Fluid Mech.* **15**, 345 (1983).
²⁰P. G. Saffman, *Vortex Dynamics* (Cambridge University Press, Cambridge, 1992), Chap. 9.
²¹D. I. Pullin, "Contour dynamics methods," *Annu. Rev. Fluid Mech.* **24**, 89 (1992).
²²G. S. Deem and N. J. Zabusky, "Vortex waves: Stationary V states, interactions, recurrence and breaking," *Phys. Rev. Lett.* **40**, 859 (1978).
²³D. G. Dritschel, "The repeated filamentation of two-dimensional vorticity interfaces," *J. Fluid Mech.* **194**, 511 (1988).
²⁴N. J. Zabusky, M. H. Hughes, and K. V. Roberts, "Contour dynamics for the Euler equations in two dimensions," *JETP* **30**, 96 (1979).
²⁵D. Durkin and J. Fajans, "Experimental dynamics of a vortex within a vortex" *Phys. Rev. Lett.* **85**, 4052 (2000).
²⁶D. Z. Jin, "Theory of vortex crystal formation in two-dimensional turbulence," Ph.D. thesis, 1999. A PDF version of the thesis can be downloaded directly from the UCSD nonneutral plasma web site, at <http://sdphca.ucsd.edu/publications.html>
²⁷D. A. Schecter, K. S. Fine, D. H. E. Dubin, and C. F. Driscoll, "Vortex crystals from 2D Euler flow: Experiment and simulation," *Phys. Fluids* **11**, 905 (1999).